Time-dependent treatment of electron-hydrogen scattering for higher angular momenta ($L>0$)

D. O. Odero,[1] J. L. Peacher,[1] D. R. Schultz,[2] and D. H. Madison[1]
[1]*Department of Physics, University of Missouri-Rolla, Rolla, Missouri 65409-0640*
[2]*Physics Division, Oak Ridge National Laboratory, Oak Ridge, Tennessee 37831-6373*
(Received 26 May 2000; published 12 January 2001)

The time-dependent approach to electron-atom scattering is emerging as an alternative to more conventional methods of treating atomic collisions. Solving the time-dependent Schrödinger equation directly has several very attractive features including a completely nonperturbative solution, dense representation of the nonphysical positive energy states, circumvention of the need to explicitly impose boundary conditions for ionization, and the convenience of being able to ''watch'' the electronic probability density evolve though the collision. Two principal approaches have so far been applied to treat electron-atom scattering, namely, the time-dependent close couping (TDCC) method and what we refer to as the time-dependent Hylleraas (TDH) method. The TDCC method solves coupled equations with two variables within a truncated infinite sum over individual angular momenta for each total angular momentum L of the system. In contrast, the TDH method avoids an infinite summation over the angular momenta of the individual electrons at the expense of solving a coupled equation with three variables for each L. The TDH method has previously been used for $L=0$ only. An important question, therefore, concerns whether the TDH method would represent a numerical advantage over the TDCC method for higher L values. This issue is investigated in this paper.

DOI: 10.1103/PhysRevA.63.022708 PACS number(s): 34.80.Dp

I. INTRODUCTION

In a theoretical treatment of an atomic collision problem, one can adopt either the time-dependent or time-independent approach. However, a particle colliding with an atom, ion or a molecule is inherently a time-dependent process in which a free particle travels towards the target and the system evolves with time under the influence of the interparticle Coulomb interactions. Such a process can be treated directly by propagating the system wave function in time according to the time-dependent Schrödinger equation. Consequently, the time-dependent approach is more closely connected to reality and it has many distinct advantages over the traditional time-independent methods. For example, it allows direct visualization of the collision process where one can ''watch'' the atom and electron wave packet evolving in time as a result of the collision. It is free of approximations (other than numerical) which means that it is inherently nonperturbative, incorporates electronic continuum states, resonances, and the postcollision interaction in the most natural way, and it circumvents the difficulty of the boundary conditions for ionization due to the long-range Coulomb interactions, which arises when using time-independent scattering theory [1]. In short, it is flexible and versatile in treating a large variety of quantum collision processes.

In addition, use of methods that solve the underlying equation of motion for electron-atom scattering, as directly as possible, are motivated by the need to try to resolve long-standing disagreements between theory and experiment for various observables that provide strenuous tests. The goal of such work is to remove uncertainties such as those arising from the use of perturbation theories when the interaction is indeed strong and the use of close-coupling theories that do not densely represent the continuum.

The general time-dependent theory of wave-packet scattering has been known for a long time [2]. However, its applications have been slow to develop due to computational (algorithmic and machine capacity) limitations. The idea behind this method is to use the time-evolution operator to evolve a known initial state into the final state. The formal solution $[\Psi(\mathbf{r}_1,\mathbf{r}_2,t+\Delta t)=e^{-\imath H\Delta t}\Psi(\mathbf{r}_1,\mathbf{r}_2,t)]$ of the time-dependent Schrödinger equation requires the representation and evaluation of the exponential time operator ($e^{-\imath H\Delta t}$) and also the formation of the initial wave function $[\Psi(\mathbf{r}_1,\mathbf{r}_2, t=0)]$ of the system. There are several formulations of the time-dependent approach for solving scattering problems [3–10] and studying the autoionization of atoms [11].

Aside from the details of the various numerical methods adopted, the most important difference between the various time-dependent approaches that have been reported so far lies in the expression for the system wave function. Perhaps the most straightforward method [6,7] is to express the system wave function as a sum over total angular momenta, where each term in this sum is a product of a coupled spherical harmonic times a function that depends on the radial coordinates for the two electrons. This approach has been termed the time-dependent close-coupling (TDCC) method [6,7]. This approach produces the usual set of coupled equations to solve, but has the disadvantage of being an infinite sum over individual angular momenta (l_1,l_2) for each total angular momentum L. Establishing that this sum is converged, when it is of necessity truncated, for each total angular momentum, represents a fundamental and numerical challenge. So far, the largest total angular momentum reported for electron-hydrogen scattering has been $L=4$. In particular, Pindzola and Robicheaux [7] calculated the partial-wave ionization cross sections for electron scattering from hydrogen using the TDCC method. In that calculation, the infinite sum was truncated after 3 terms for total $L=0$, 6 terms for $L=1$ and $L=2$, and 8 terms for $L=3$ and 4.

The alternative approach, which has been developed by Bottcher *et al.* [11–15], is to express the wave function for a

given total angular momentum as a product of a coupled spherical harmonic times a function that depends on the radial coordinates for the two electrons as well as the angular separation between the two electrons. The basis for this method has been attributed to Hylleraas [16] and is therefore called the time-dependent Hylleraas (TDH) method, and has the distinct advantage of being a *finite* sum for each total angular momentum L with either L or $(L+1)$ terms depending on the parity of the initial state. The disadvantage of this method lies in the fact that there are now three dynamical variables for the system and, as a result, the matrices representing the various operators are three-dimensional, which severely limits the possible size for each dimension. Consequently, the TDH method poses a potentially much greater numerical challenge than the TDCC method. Thus, the two presently developed options for treating electron-atom scattering by direct solution of the Schrödinger equation are (1) choose an easier computational problem but perform a truncated ''infinite'' summation over the individual (l_1,l_2) for each total angular momentum, or (2) solve a more difficult computational problem but with a small finite sum over the individual $(l_1,\ l_2)$ for each total angular momentum. The TDH method has previously been applied to electron-hydrogen scattering for total $L=0$ only [3]. The purpose of this paper is to use the TDH method to calculate higher L-value results for electron-hydrogen scattering to determine which option is the more viable and/or practical. In the current approach, the basis-spline collocation method [17–19] is used to represent the operators and to discretize the wave functions on the grid and the time-evolution operator is evaluated using a Taylor series method as described in Buffington *et al.* [3]

II. THEORY OF ELECTRON-HYDROGEN ATOM COLLISION

The theory has previously been presented in Buffington *et al.* [3] and Schultz *et al.* [11] so only the essential points will be given here. The time-dependent Schrödinger equation for the wave function $\Psi(\mathbf{r}_1,\mathbf{r}_2,t)$ describing the electron-hydrogen atom system has the general form

$$H\Psi(\mathbf{r}_1,\mathbf{r}_2,t)=\imath\frac{\partial}{\partial t}\Psi(\mathbf{r}_1,\mathbf{r}_2,t). \tag{1}$$

Atomic units are used unless stated otherwise. The Hamiltonian H for a system containing a nucleus and two electrons can be expressed in atomic units (a.u.) as

$$H=-\frac{1}{2}(\nabla_1^2+\nabla_2^2)-\frac{q}{r_1}-\frac{q}{r_2}+\frac{1}{|\mathbf{r}_1-\mathbf{r}_2|}, \tag{2}$$

where q is the charge of the nucleus and the vectors $\mathbf{r}_1$ and $\mathbf{r}_2$ locate the electrons with respect to the assumed infinitely massive nucleus, which is fixed at the origin.

For a fixed total angular momentum L, projection M, and parity ϖ, the wave function in Eq. (1) can be written in terms of an expansion attributed to Hylleraas [3,11,16] as

$$\Psi_{\varpi}^{LM}(\mathbf{r}_1,\mathbf{r}_2,t)=\frac{1}{r_1r_2}\sum_{l_1=\varpi}^{L}\psi_{l_1}(r_1,r_2,\vartheta,t)\mathcal{Y}_{l_1,L+\varpi-l_1}^{LM}(\hat{r}_1,\hat{r}_2). \tag{3}$$

The expansion coefficient ψ_{l_1} is referred to as the dynamical wave function and ϑ is the angle between $\mathbf{r}_1$ and $\mathbf{r}_2$. The parity $\varpi=0$ or 1 depending on whether the wave function exhibits even (natural) or odd (unnatural) parity [15]. For the collision system considered here, the wave function exhibits even parity, so $\varpi=0$. Consequently, for a given total angular momentum L, there are $(L+1)$ dynamical wave functions.

The dynamical wave functions ψ_{l_1} satisfy the coupled [3,15,11] equations

$$\left(h_1+h_2+h_\vartheta+\frac{1}{r_{12}}-E\right)\psi_{l_1}+\sum_{l_1'=\varpi}^{L}[\mathcal{U}_{ll'}^{(1)}(\vartheta)+\mathcal{U}_{ll'}^{(2)}(\vartheta)]\psi_{l_1'}=0, \tag{4}$$

where, for convenience, the shorthand notation $l=(l_1,l_2)=(l_1,L+\varpi-l_1)$ and $l'=(l_1',l_2')=(l_1',L+\varpi-l_1')$ is used,

$$\begin{aligned}h_1&=-\frac{1}{2}\frac{\partial^2}{\partial r_1^2}-\frac{q}{r_1}+\frac{l_1(l_1+1)}{2r_1^2},\\ h_2&=-\frac{1}{2}\frac{\partial^2}{\partial r_2^2}-\frac{q}{r_2}+\frac{l_2(l_2+1)}{2r_2^2},\\ h_\vartheta&=-\frac{1}{2}\left(\frac{1}{r_1^2}+\frac{1}{r_2^2}\right)\mathcal{D}_\vartheta[\sin^2\vartheta\mathcal{D}_\vartheta]\end{aligned} \tag{5}$$

and the coupling terms are given by

$$\begin{aligned}\mathcal{U}_{ll'}^{(p)}&\equiv-\frac{\mathcal{Z}_{ll'}^{(p)}}{\mathcal{Z}_{ll'}^{(0)}}\frac{1}{r_p^2}\mathcal{D}_\vartheta,\quad p=1,2,\\ \mathcal{D}_\vartheta&=\frac{1}{\sin\vartheta}\frac{\partial}{\partial\vartheta}.\end{aligned} \tag{6}$$

The $\mathcal{Z}$ matrices are composed of Legendre polynomials, Clebsch-Gordan coefficients, and Racah coefficients. Explicit expressions for the $\mathcal{Z}$ matrices are given in Ref. [15]. They give rise to the mixing of the dynamical wave functions.

Initially the electron-electron interaction can be ignored since the electrons are far apart. The initial wave function in Eq. (1) consists of the initial atomic state and incident electron, which is represented by an incoming spherical wave. The initial angular-independent dynamical wave functions become angularly dependent as the time-propagation progresses. For a state with zero total angular momentum $(L=0)$, the initial singlet or triplet $(S=0$ or 1) wave function would be given by

$$\psi_{l_1=L=0}(r_1,r_2,\vartheta,t=0)$$

$$=\frac{1}{\sqrt{2}}[\phi_{l_1=0}(r_1)\chi_{l_2=\varpi}(r_2)$$

$$+(-1)^{S+\varpi}\phi_{l_1=0}(r_2)\chi_{l_2=\varpi}(r_1)], \qquad (7)$$

where, in general, $l_2=L+\varpi-l_1$. As noted previously $\varpi=0$ for this collision system. Here, ϕ would represent the ground state of hydrogen and χ the incoming projectile electron wave packet.

For states with total angular momentum greater than zero, the initial dynamical wave functions are given by

$$\psi_{l_1=0}(r_1,r_2,\vartheta,t=0)=\frac{1}{\sqrt{2}}\phi_{l_1=0}(r_1)\chi_{l_2=L}(r_2),$$

$$\psi_{l_1=L}(r_1,r_2,\vartheta,t=0)=\frac{1}{\sqrt{2}}(-1)^{S+\varpi}\phi_{l_1=L}(r_2)\chi_{l_2=\varpi}(r_1), \qquad (8)$$

$$\psi_{l_1}(r_1,r_2,\vartheta,t=0)=0, \quad l_1\neq 0, \quad \text{and} \quad l_1\neq L.$$

The incoming projectile wave packet is given by

$$\chi_{l_2}(r)=\frac{-ikr}{(\pi b^2)^{1/4}}h_{l_2}^{(-)}(kr)\exp\left[-\frac{1}{2}\left(\frac{r-a}{b}\right)^2\right], \qquad (9)$$

where $h_{l_2}^{(-)}(kr)$ is an incoming spherical Hankel function, k is the momentum of the projectile electron, a is the initial center of the Gaussian wave packet, while b defines its width. Although it would appear that the singlet and triplet wave functions would both need to be propagated independently, the indistinguishability of the two electrons makes it possible to propagate only a single wave function that can be used to get both the singlet and triplet results.

The propagation proceeds according to the equation

$$\Psi^{LM}(\mathbf{r}_1,\mathbf{r}_2,t+\Delta t)=e^{-\imath H\Delta t}\Psi^{LM}(\mathbf{r}_1,\mathbf{r}_2,t). \qquad (10)$$

The time evolution operator ($e^{-\imath H\Delta t}$) is evaluated using the Taylor series expansion

$$e^{-\imath H\Delta t}=\sum_N \frac{(-\imath H\Delta t)^N}{N!}. \qquad (11)$$

The time-dependent probability of finding one electron in the bound state nlm of hydrogen and the other electron in the continuum, i.e. the excitation probability, is given by [3,5]

$$P_{nlm}^{LM}(t)=2\left[\wp_{nlm}^{LM}(t)-\sum_{n'l'm'}\wp_{nlm,n'l'm'}^{LM}(t)\right]. \qquad (12)$$

Here $\wp_{nlm}$ is the probability that one electron is in the bound state nlm, while the other electron is in any bound or continuum state and $\wp_{nlm,n'l'm'}$ is the probability that one electron is in the bound state nlm while the other electron is in the bound state $n'l'm'$. The factor of two accounts for the indistinguishability of the electrons.

The one-electron probability $\wp_{nlm}^{LM}$ may be obtained by projecting the single-particle state onto the full wave function

$$\wp_{nlm}^{LM}(t)=\int |\langle\langle \phi_{nlm}(\mathbf{r}_1)|\Psi^{LM}(\mathbf{r}_1,\mathbf{r}_2,t)\rangle\rangle|^2\, d\mathbf{r}_2, \qquad (13)$$

where $\phi(\mathbf{r}_1)$ describes a possible one-electron bound state of the atom, $\Psi^{LM}(\mathbf{r}_1,\mathbf{r}_2,t)$ is the fully correlated time-dependent wave function for the two-electron system, and the double brackets indicate integration over $\boldsymbol{r}_1$. Equation (13) represents the probability that one electron is in the nlm state while the other could be in any possible state. The two-electron probability $\wp_{nlm,n'l'm'}^{LM}$ is defined by the projection

$$\wp_{nlm,n'l'm'}^{LM}(t)=|\langle \phi_{nlm}(\mathbf{r}_1)\phi_{n'l'm'}(\mathbf{r}_2)|\Psi^{LM}(\mathbf{r}_1,\mathbf{r}_2,t)\rangle|^2, \qquad (14)$$

where now the integration is over both $\boldsymbol{r}_1$ and $\boldsymbol{r}_2$. Expression (14) represents the probability that one electron is in the nlm state and the other electron is in the $n'l'm'$ state. The probabilities are monitored as the time evolution continues to large times until the probabilities reach their asymptotic values. The inelastic excitation cross sections can be obtained from [5,6]

$$\sigma_{nl}^{LM}=\frac{\pi}{4k^2}\sum_m (2S+1)(2L+1)P_{nlm}^{LM}, \qquad (15)$$

where k is the momentum of the incident electron.

The excitation probabilities are extracted at a final time such that the outgoing wave packet is far from the scattering atom and the grid boundaries. To verify the numerical procedures adopted, the normalization of the wave function and the total energy of the system were monitored as a function of time. These did not change with time either in the presence or absence of the scattering potential.

III. RESULTS

A. Numerical parameters

The only approximations which are made in this paper are numerical and we have used the basis-spline collocation method to represent our dynamical wave functions. To implement this method, one must choose a spline order, a numerical grid for r_1, r_2, and ϑ, the time step Δt, the initial location for the incoming wave packet, and the width of the wave packet. We have used splines of order 3. The choice for Δt represents a trade off between propagation time and the number of terms required for convergence of the Taylor series of Eq. (11). A large time step will reduce the number of terms required to reach the asymptotic limit but for each time step, the series of Eq. (11) will converge slower and thus require more terms. We performed a systematic study of these competing factors and found that $\Delta t=0.005$ a.u. represented an optimum compromise for our chosen grids.

The parameters for the wave packet were chosen to satisfy certain criteria. The wave packet should be narrow and

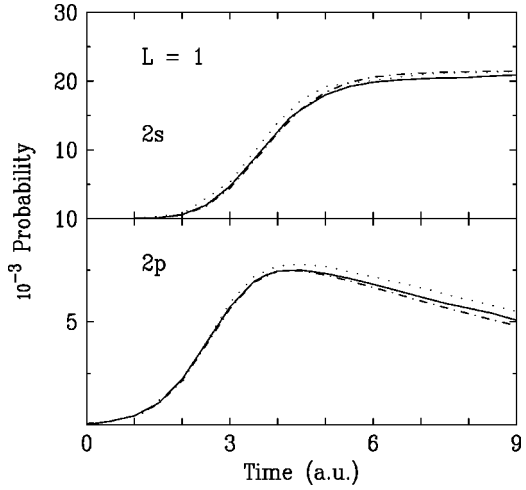

FIG. 1. Time-dependent probabilities for exciting the $n=2$ singlet states for $L=1$ at 100-eV electron impact energy. The various curves are for different box size and number of points: dotted, 25/60, solid, 30/60, and dot dashed, 30/80.

yet at the same time have a minimum amount of spreading. For the energies considered here a width of $b=3$ a.u. satisfied this criterion and was also consistent with previous time-dependent calculations [3,6]. For the location of the incoming wave packet, the criterion is to start far enough out so that there is little interaction between the two electrons. On the other hand, one does not want to start too far out since propagating with no interaction would consume computer time and have no effect other than the spreading of the wave packet. We tested various starting points and found that placing the center of the wave packet at 10 a.u. represented a good compromise.

The last choice that must be made is the spacing of the basis spline points of support (or of collocation) on the numerical grids for the radial and angular coordinates. The angular coordinate must necessarily span the range of zero to π and we found that 12 angular grid points were sufficient. Probably the most important choice to be made is the representation of the r_1 and r_2 grids. Due to the indistinguishability of the two electrons, the same grids were used for both electrons. In principle, these grids extend from zero to infinity. In practice one must chose a maximum value. Consequently, the necessary choices are the maximum value for the radial grid (box size) and the number of points inside the box (which corresponds to the number of basis splines for each coordinate, and therefore, the subrank of the Hamiltonian matrix). Below we designate a box with maximum size M a.u. with N points inside the box as ''M/N.''

To determine the optimum box size and number of points, we performed a series of calculations for different choices. It is desirable to perform the tests for the smallest L value since the run time increases dramatically with L value (and, therefore, number of coupled equations to be solved). Consequently, the tests were performed for $L=1$ since this is the smallest L value for which the coupling terms contribute. In Figs. 1 and 2, the probability for exciting the $n=2$ and 3 levels are shown as a function of time for boxes 25/60, 30/60, and 30/80. This comparison was performed for a 100-eV

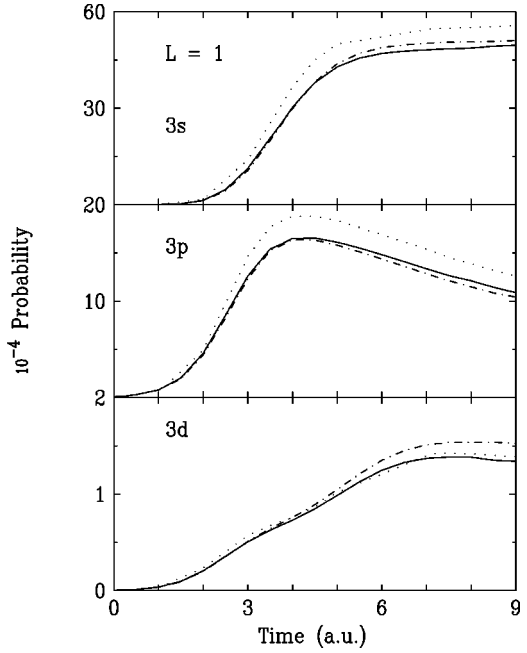

FIG. 2. The same as Fig. 1 except for excitation to the $n=3$ singlet state.

incident electronic wave packet and a total spin of zero. Triplet results are very similar and not shown for brevity. In general, we found that when the different grids produced significantly different results, the two calculations for box size 30 a.u. tended to be very similar to each other and noticeably different from the box size of 25 a.u. (even when the same number of points are used). The explanation for this observation can be found by looking at the atomic wave functions. The $2s$ wave function as well as the $2p$ wave function are well within the 25 a.u. box while the $n=3$ wave functions extend beyond 25 a.u. These results reflect the obvious fact that accurate results for exciting a particular atomic wave function requires a box at least as large as the state of interest. The similarity of the 30/60 and 30/80 results indicates that the density-of-states is less important than box size. Consequently, 30/60 was chosen as the radial grid for this study. From Fig. 2 it is seen that the largest difference between the 30/60 and 30/80 results was found for the $3d$ state. The fact that the 25/60 and 30/60 results for the $3d$ state are very similar is undoubtedly fortuitous. Cross sections for this state will therefore have the largest numerical errors. Convergence of the excitation cross sections is determined by continuation of the time evolution until the probabilities have reached their asymptotic values (somewhat larger times than those shown in Figs. 1 and 2).

B. Inelastic excitation probabilities

The time-dependent excitation probabilities are calculated from the time-dependent wave functions using Eq. (12). As mentioned in the previous section, these probabilities must have reached their asymptotic values before one can obtain meaningful cross sections. Figure 3 shows the 30/60, $n=2$ probabilities for times up to 15 a.u. It is seen that both the $2s$ and $2p$ probabilities are at their asymptotic values after 12

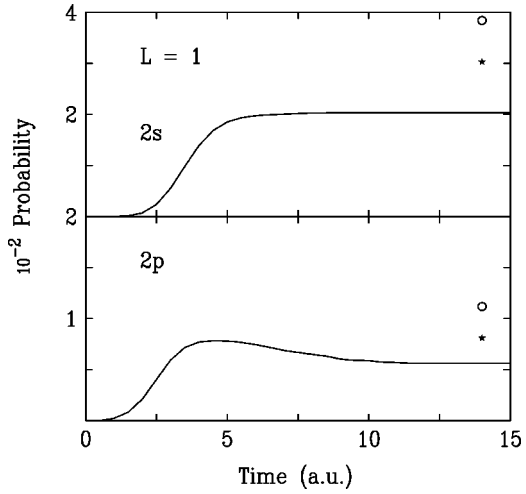

FIG. 3. Time-dependent probabilities for exciting the $n=2$ singlet states for $L=1$ at 100-eV electron impact energy. Solid line, 30/60 TDH results; circles, DWB2 results (Ref. [20]), and stars, CCC results (Ref. [21]).

a.u. The probabilities for the $n=3$ states are not displayed since all the n bound states as well as all the L values considered here exhibited very similar behavior. The purpose of Fig. 3 is to demonstrate that the probabilities reach their asymptotic values with increasing time and this happens for all the states we examined. Also shown in Fig. 3 are the exact second-order distorted wave-Born (DWB2) approximation of Madison *et al.* [20] and the convergent close-coupling (CCC) results of Bray and Stelbovics [21,22]. These are time-independent calculations and are placed at a large time value since they should represent the asymptotic value for a time-dependent calculation. It is seen that the CCC results are closer to the present TDH results than to the DWB2 results for this case.

C. Excitation cross sections

Cross sections for exciting the $2s$, $2p$, $3s$, $3p$, and $3d$ states of hydrogen by electron impact at seven energies between 30 and 122.5 eV have been calculated for total angular momenta, L between 0 and 3. The results are displayed in Figs. 4 through 8. All calculations have been carried out on small or midlevel workstations such as the HP 9000/715 or SGI Power Challenge. Typical run times for total angular momentum $L=0$ ranged between 1 week for the highest incident energy considered here (122.5 eV) to two weeks for 30 eV for the 30/60 box. The run time increases dramatically with higher angular momentum (and thus more coupled equations) and means to parallelize the algorithms to take advantage of contemporary multicomputers is prudent if further work, utilizing the TDH method, is to be performed.

For comparison the analogous DWB2 [20] and CCC [21,22] cross sections have been computed. It would, of course, also be instructive to compare the TDH results for excitation directly with the TDCC results but only ionization cross sections were reported in Ref. [7]. Fortunately, the CCC and DWB2 results are generally expected to be representative of the present state of the art for nonperturbative

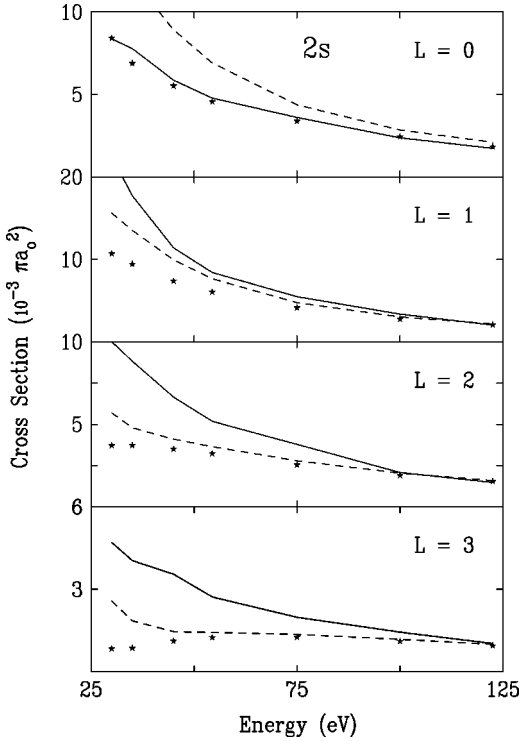

FIG. 4. Cross sections for electron-impact excitation of the $2s$ state of atomic hydrogen for total angular momenta between 0 and 3 as a function of the incident electron energy. The cross sections have been summed over the individual singlet and triplet contributions. The theoretical results are as follows: solid curve, present 30/60 TDH results, stars, CCC results (Ref. [21]), and dashed curve, DWB2 results (Ref. [20]).

treatments for total excitation cross sections. The $L=0$ singlet and triplet results were presented elsewhere [3] but the total results are presented here for completeness. The present TDH results for $L=0$ agree very nicely with the CCC results for all the excited states and energies considered. For $L=0$, the DWB2 approximation, on the other hand, tends to be above the other theories at low energy for s- and p-state excitation and below the other theories for d-state excitation. All the theories converge at higher energies for all L values.

For $2s$ excitation (Fig. 4), all three theoretical approaches predict very similar results for energies of 100 eV and above. For $L=0$, there is good agreement between the present results and the CCC at all energies considered. For higher L values and lower energies, the present TDH results are larger than either the CCC or DWB2 results while the latter two theories are in reasonable agreement with each other except at the lowest energies. For $2p$ excitation (Fig. 5), on the other hand, the situation is quite different in that the present TDH results are in good agreement with the CCC results at all energies for L values of 0, 1, and 2 and in fair agreement for $L=3$. In this case, the DWB2 results tend to be larger than the other two theories at low energies which can be explained by the fact that the DWB2 calculation is expected to be valid for higher energies. With decreasing energy, the DWB2 calculation is expected to become less reliable as third- and higher-order terms become more important. Consequently, the $2p$ results are consistent with what one would

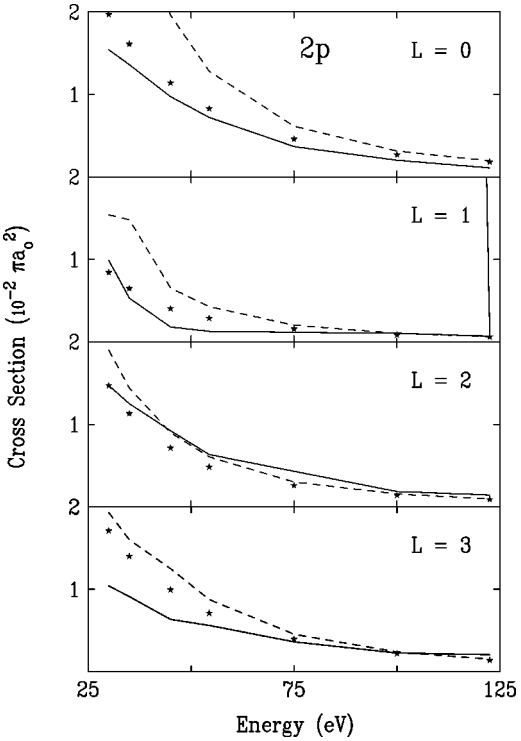

FIG. 5. Same as Fig. 4 except for the $2p$ state.

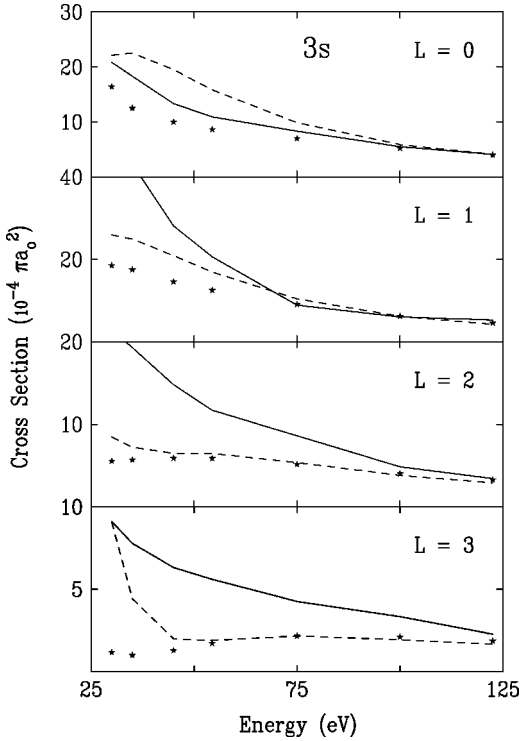

FIG. 6. Same as Fig. 4 except for the $3s$ state.

naively expect to find while the $2s$ results are not. It is then logical to question the validity of the $2s$ results. The first thing that comes to mind is numerical accuracy, particularly since the radial grid is relatively sparse (60 points). If the $2s$ cross sections were significantly smaller than the $2p$ cross sections, for example, one could argue that the cross sections were too small to be accurately calculated using this radial grid. Unfortunately, this argument does not explain the present results since the TDH $L=1$ cross section is larger for $2s$ than for $2p$ excitation and for $L=2$, the $2s$ and $2p$ cross sections are comparable in size. Further, the theories converge for the higher energies for all L values, where the cross sections tend to be the smallest. Consequently, the unexpected behavior of the $2s$ results cannot be explained by arguing that the cross sections are too small to be accurately predicted by the present numerical grid.

Figures 6 and 7 present results for excitation of the $3s$ and $3p$ states. The $3s$ results are very similar to the 2s results. The only striking difference between the $2s$ and $3s$ results lies in the fact that the TDH and DWB2 results are nearly identical at the lowest energy for $L=3$. This is undoubtedly coincidental since the DWB2 calculation is not expected to be valid for low energies. The $2p$ and $3p$ results are also very similar. The present TDH results are in reasonably good agreement with the CCC results for $3p$ excitation in spite of the fact that the $3p$ cross sections are about a factor of 5 smaller than the corresponding $2p$ cross sections. The only exception lies in the fact that the agreement is not good for $L=3$ at smaller energies and this disagreement is worse for $3p$ than for $2p$.

Finally, the results for $3d$ excitation are shown in Fig. 8. As mentioned above, we expect the $3d$ results to be the least reliable for the chosen numerical grid. Here we again see very good agreement between the TDH and CCC results for $L=0$ and all theories are converging at the higher energies. For the lower energies, the DWB2 and CCC results are in reasonable agreement while the TDH results are smaller than the other theories for $L>0$.

In summary, the present TDH results are difficult to understand. Both the TDH and CCC calculations are nonper-

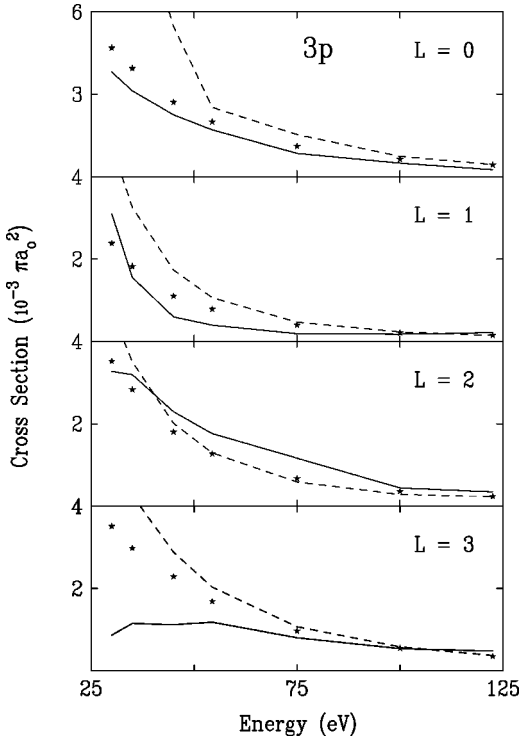

FIG. 7. Same as Fig. 4 except for the $3p$ state.

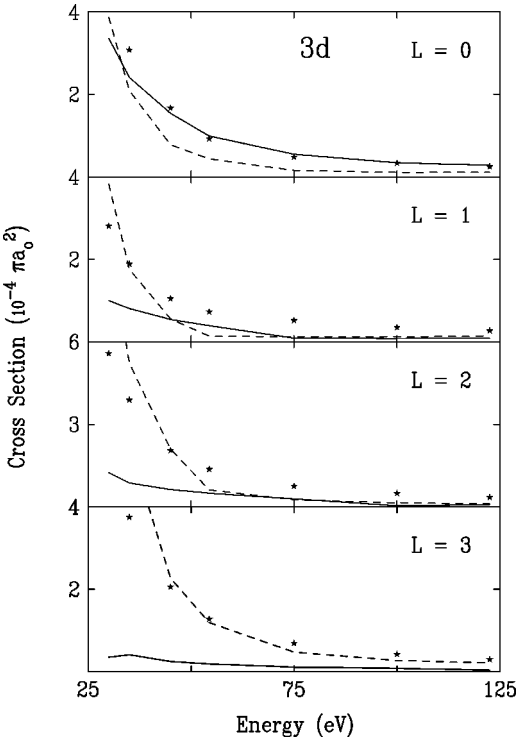

FIG. 8. Same as Fig. 4 except for the 3*d* state.

turbative and one would expect that they should yield identical (and accurate) results if there is proper numerical convergence. The CCC results are in good agreement with absolute experimental data for differential cross sections and total cross sections in this energy range (i.e., present results summed over all L values) so there is no reason to suspect a problem with the CCC calculation. The CCC and TDH results agree well for $L=0$ over the entire energy range. However with increasing L values, good agreement is found only for *p* states and even in this best case the agreement begins to break down for the highest L value of 3 considered here. The primary question thus concerns the source of this seemingly paradoxical situation.

The most obvious possibility is an inadequate radial grid in the TDH calculation. The grid tests were performed for $L=1$ (these runs take about 3 weeks for 60 grid points). Since the disagreement with the CCC calculation gets worse with increasing L value, it is possible that sensitivity to the grid increases with increasing L value. Consequently, we performed a 30/60, 30/80, and 40/80 grid test calculation for $L=3$. These calculations took several months to complete. The results of these calculations for $n=2$ and 3 are shown in Figs. 9 and 10, respectively, and indicate that the problem is not in the box size nor grid density.

Since all the theoretical results are in good agreement for $L=0$, one might speculate that the difference in the TDH results for higher L values might be due to the coupling matrices, which do not contribute for $L=0$. From Eq. (6), it is seen that the coupling terms involve inversion of the $\mathcal{Z}^{(0)}_{l'l}(\vartheta)$ matrices and the stability of this procedure could play an important role. The $\mathcal{Z}^{(0)}_{l'l}(\vartheta)$ of Eq. (6) are expanded in terms of Legendre polynomials as

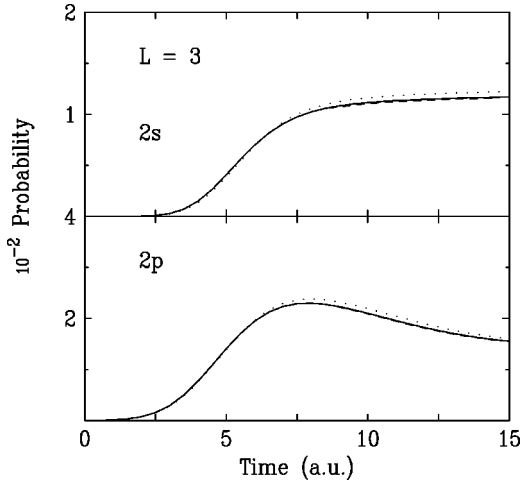

FIG. 9. Time-dependent probabilities for exciting the $n=2$ singlet states for $L=3$ at 54.4-eV electron impact energy. The various curves are for different box size and number of points: solid, 30/60, dotted, 30/80, and dashed, 40/80.

$$\mathcal{Z}^{(0)}_{l'l}(\vartheta)=\sum_k \mathcal{Z}^{(0)}_{kLl'l}P_k(\cos\vartheta). \tag{16}$$

The expansion coefficients for Eq. (16) can be written as follows [3]

$$\mathcal{Z}^{(0)}_{kLl'l}=\frac{1}{2}(-1)^{k+L}\sqrt{(2l_1+1)(2l_1'+1)(2l_2+1)(2l_2'+1)}\times C(l_1l_1'k;0,0,0)C(l_2l_2'k;0,0,0)W(l_1l_1'l_2l_2';kL), \tag{17}$$

where C is a Clebsch–Gordan coefficient and W is a Racah coefficient.

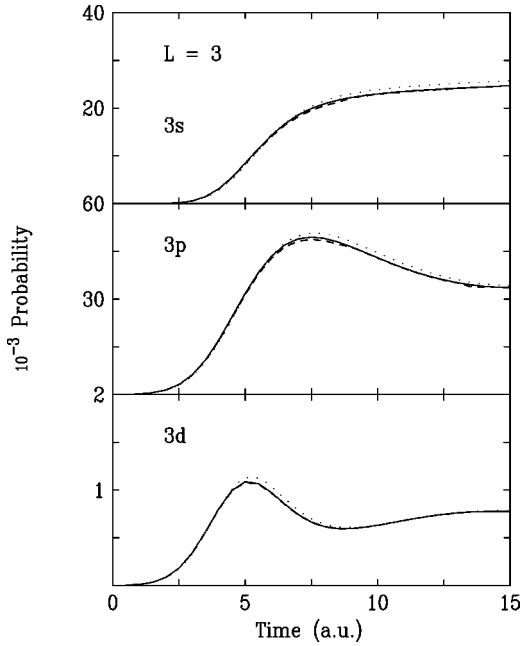

FIG. 10. Same as Fig. 9 except for excitation to the $n=3$ singlet states.

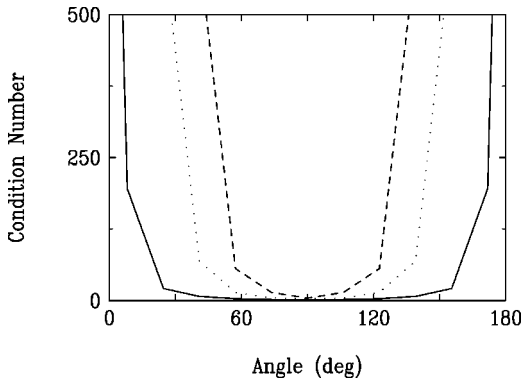

FIG. 11. Condition number for the $\mathcal{Z}^{(0)}_{ll'}(\theta)$ coupling matrices as a function of the angle between the two electrons. The curves are for different total angular momenta: solid, $L=1$, dotted, $L=2$, and dashed, $L=3$.

To check the stability of the inversion of this matrix, the condition number was computed for the $\mathcal{Z}^{(0)}_{ll'}(\vartheta)$ matrix for different L values as a function of angle. The condition number is the ratio of the largest eigenvalue to the smallest eigenvalue for the matrix. The larger the ratio the more nearly singular is the matrix and the less stable (or reliable) is the inversion of the matrix. Figure 11 shows the condition number as a function of the angle between the two particles. The solid line represents the condition number for $L=1$, dotted $L=2$, while the dashed line is for $L=3$. It is observed that the condition number is very large for angles near 0° and 180° and that the region of stability decreases with increasing L value. The matrix inversion is most stable near 90° and the condition number is symmetric about 90°. From Fig. 11, it can be seen that for different L values, there are characteristic angular ranges for which the inverses of the $\mathcal{Z}^{(0)}_{ll'}(\vartheta)$ matrices are stable and these ranges decrease with increasing L values. This implies that the solution of the coupled equations will potentially have stability problems near 0° and 180°, which become more severe with increasing L. The stability problems associated with the $\mathcal{Z}^{(0)}_{ll'}(\vartheta)$ matrix near 0^o and 180^o means that one must be very careful with the numerical method used to take the inverse, particularly for increasing L. For this paper, the direct methods [23] (Gaussian elimination, Gaussian elimination with partial pivoting, Gaussian elimination with full pivoting, and Gauss-Jordan) were tested. The first important issue concerns how one can evaluate the reliability and accuracy of different methods for taking inverses. In principle, it would seem that the accuracy of an inverse could easily be tested by checking the multiplication of the original matrix by its inverse. However, for nearly singular matrices, this test is highly sensitive to the number of significant digits used and changing the least significant digit by one can produce dramatic changes.

One important check of the inverse lies in the fundamental physics. The inverse of the $\mathcal{Z}^{(0)}_{ll'}(\vartheta)$ matrix determines the coupling between the individual angular momenta in the total wave function. With time propagation, the norm and energy of the total wave function must be constant. As a result, any procedure for taking the inverse that does not conserve the norm and the energy is clearly unreliable. Of all the methods we tested for taking the inverse, only the Gauss-Jordan method conserved both the energy and norm. Consequently, this is the method we have used in the present work. Admittedly, this test is necessary but may not be sufficient. Although the norm and energy were conserved for all the results shown here, we believe that the instability in inverting this matrix is the most likely source for the difference between the TDH and CCC calculations for increasing L values.

IV. CONCLUSION

We have calculated TDH results for electron impact excitation of hydrogen for total angular momenta 0 to 3. The present TDH approach has the distinct advantage over other time-dependent approaches such as the TDCC method of Pindzola and Robicheaux [7] in that the sum over the individual (l_1, l_2) is finite and can be performed exactly, while in the TDCC method this sum is infinite and must be truncated. Consequently, a primary motivation for this paper has been to test the feasibility and practicality of the TDH method for higher L values. Our main conclusion is that while the TDH does appear to provide a straightforward pathway to a direct, fully-correlated treatment of electron-atom scattering, it is not presently implemented in a manner that makes it a practical alternative to the lower-dimensional, parallelizable TDCC method. Aside from the very long run times, the coupling terms in the TDH method involve taking the inverse of a matrix, which is nearly singular for small and large angular separations and the instability for this matrix inversion increases with increasing L values. The fact that the present results do not agree with the CCC results strongly suggests that this instability has caused inaccuracies in the present results, particularly for excitation of non-p states (and even p states for higher angular momenta). Therefore, the future applicability, utility, and feasibility of the TDH approach for L greater than zero critically depends on its reformulation in such a way as to avoid taking the inverse of the $\mathcal{Z}^{(0)}_{ll'}(\theta)$ matrix or development of a stable inversion procedure and the speeding up of computational turn-around time through development of a parallelization scheme for the method.

ACKNOWLEDGMENTS

D.O.O., D.H.M., and J.L.P. gratefully acknowledge support from the NSF. Work by D.R.S. was supported through grants to the Oak Ridge National Laboratory, managed by UT-Battelle, LLC under Contract No. DE-AC05-00OR22725 from the U.S. DOE Office of Fusion Energy Sciences and Office of Basic Energy Sciences.

[1]

[1] J. Berakdar and H. Klar, J. Phys. B **26**, L4219 (1993).
[2] M.L. Goldberger and K.M. Watson, *Collision Theory* (Wiley, New York, 1964).
[3] G.D. Buffington, D.H. Madison, J.L. Peacher, and D.R. Schultz, J. Phys. B **32**, 2991 (1999).
[4] D. Kato and S. Watanabe, Phys. Rev. Lett. **74**, 2443 (1995).
[5] W. Ihra, M. Draeger, G. Handke, and H. Friedrich, Phys. Rev. A **52**, 3752 (1995).
[6] M.S. Pindzola and D.R. Schultz, Phys. Rev. A **53**, 1525 (1996).
[7] M.S. Pindzola and F. Robicheaux, Phys. Rev. A **54**, 2142 (1996).
[8] M.S. Pindzola and F. Robicheaux, Phys. Rev. A **61**, 052707 (2000).
[9] M.S. Pindzola, D.M. Mitnik, J. Colgan, and D.C. Griffin, Phys. Rev. A **61**, 052712 (2000).
[10] A. B. Ritchie and C. A. Weatherford, Int. J. Quantum Chem. **80**, 934 (2000).
[11] D.R. Schultz, C. Bottcher, D.H. Madison, J.L. Peacher, G. Buffington, M.S. Pindzola, T.W. Gorczyca, P. Gavras, and D.C. Griffin, Phys. Rev. A **50**, 1348 (1994).
[12] C. Bottcher, J. Phys. B **14**, L349 (1981).
[13] C. Bottcher, J. Phys. B **15**, L463 (1982).
[14] C. Bottcher, Adv. At. Mol. Phys. **20**, 241 (1985).
[15] C. Bottcher, D.R. Schultz, and D.H. Madison, Phys. Rev. A **49**, 1714 (1994).
[16] E.A. Hylleraas, Z. Phys. **48**, 469 (1928).
[17] A.S. Umar, J.S. Wu, M.R. Strayer, and C. Bottcher, J. Comput. Phys. **93**, 426 (1991).
[18] C. de Boor, *A Practical Guide to Splines* (Springer-Verlag, New York, 1978).
[19] P.M. Prenter, *Splines and Variational Methods* (Wiley, New York, 1975).
[20] D.H. Madison, I. Bray, and I. McCarthy, J. Phys. B **24**, 3861 (1991).
[21] I. Bray and A.T. Stelbovics, Phys. Rev. A **46**, 6995 (1992).
[22] I. Bray and A.T. Stelbovics, Adv. At. Mol. Phys. **35**, 209 (1995).
[23] T.R. McCalla, *Introduction to Numerical Methods and* FORTRAN *Programming* (Wiley, New York, 1967).